

# Numerical analysis of a toroidal rotation effect on the type-I ELM in JT-60U

N. Aiba, N. Oyama, A. Kojima, S. Tokuda<sup>1)</sup>

*Japan Atomic Energy Agency, Naka 311-0193, Japan*

<sup>1)</sup>*Research Organization for Information Science and Technology, Tokai 319-1106, Japan*

(Received: 26 October 2009 / Accepted: 23 February 2010)

Effect of a toroidal rotation on the type-I edge localized mode in JT-60U is investigated numerically. As the result of the numerical analysis, it is confirmed that the plasma rotating experimentally in the co-direction to the plasma current is approximately on the stability boundary of the MHD mode even when the rotation is neglected. However, the plasma rotating in the counter-direction is far from the stability boundary under the static assumption. Since both plasmas have the type-I ELM, the edge MHD stability is reassessed with the toroidal rotation effect. This stability analysis clarifies that the rotation of this counter rotating plasma can destabilize the edge localized MHD mode, and can resolve the discrepancy that the type-I ELM is observed in the plasma that is MHD-stable under the static assumption.

Keywords: ELM, ideal MHD stability, toroidal rotation, Frieman-Rosenbluth equation

## 1. Introduction

In tokamak plasmas, a transport barrier sometimes appears near the plasma surface, and makes a pedestal structure in the plasma density and the temperature profiles. The plasma with such pedestal structures, called H-mode, is favorable to improve a energy confinement, which is enough to reach burning plasma conditions. In such H-mode plasmas, edge localized modes (ELMs) are usually observed, and constrain the maximum pressure gradient in the pedestal [1].

The recent experimental results in JT-60U show that the plasma toroidal rotation at the pedestal has an impact on the ELM phenomena [2, 3]. However, this dependence of the ELM phenomena on the toroidal rotation is complicated to understand only with the experimental results. In fact, the toroidal rotation can change not only the ELM phenomena but also the equilibrium pressure (density, temperature) profile near the pedestal, and it is difficult to identify whether the transport property or the stability property is responsible for this change of the pedestal profile. For comprehending such a complicated dependence between the ELM phenomena and the plasma rotation, it is necessary to understand the physics with the theoretical and numerical analyses.

Previous numerical and experimental works have reported that the ideal MHD modes destabilized near the plasma surface, called the peeling-ballooning mode, is thought to be responsible for the type-I ELM [1, 4]. On the basis of this result, we investigated the toroidal rotation effect on the ideal MHD modes at tokamak edge pedestal, and reported that the edge localized MHD mode can be destabilized by the toroidal rotation with shear though the ballooning mode stability changes little [5]; an other paper also reported that the toroidal rotation shear increase the growth rate of intermediate wave length MHD modes [6].

In Ref. [7], furthermore, we have clarified that this destabilization is mainly caused by the difference between the frequency of the eigenmode and the toroidal rotation frequency, and this effect becomes effective only when the rotation profile has large shear in the radial direction.

Based on these results, in this paper, we investigate numerically the effect of the toroidal rotation on the type-I ELM in JT-60U. Fortunately, in the last campaign of JT-60U, several diagnostics were installed so as to obtain high spatial resolution profiles near the pedestal, and realize to analyze the edge MHD stability with high accuracy.

This paper is organized as follows. Section 2 introduces the profiles of the toroidally rotating equilibria reconstructed with the experimental data of the JT-60U type-I ELMy H-mode plasmas. Section 3 shows the numerical results of the stability analysis in not only the rotating but also the static cases. By comparing the results in both cases, we discuss the toroidal rotation effect on the type-I ELM in JT-60U. Section 4 presents a summary of this work.

## 2. Equilibrium profiles

The equilibria analyzed numerically are obtained by the reconstruction with the experimental data of the E49228 and the E49229 plasmas in JT-60U; the details of these plasmas are shown in Ref. [8]. As discussed in Ref. [8], these plasmas have the same toroidal magnetic field  $B_{t0} = 4.0$ [T] and plasma current  $I_p = 1.6$ [MA], but the plasma rotation profiles are different between E49228 and E49229, whose toroidal rotation are in the co-(CO.) and ctr-(CTR.) directions to the plasma current, respectively. Such a difference of the rotation profiles are due to changing the combination of the momentum input with neutral beam injection (NBI). By changing the rotation profile from CO. to CTR., the type-I ELM frequency increases from  $\sim 37$ [Hz] to  $\sim 45$ [Hz], and the ELM energy

author's e-mail: aiba.nobuyuki@jaea.go.jp

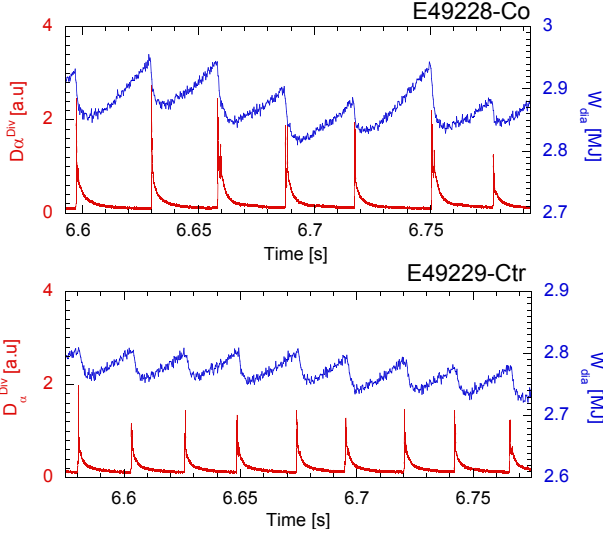


Fig. 1 Waveforms of the E49228 (CO.) and the E49229 (CTR.) plasmas, which are rotating in the co- and the ctr-directions, respectively. The red line and the blue line show the divertor  $D_\alpha$  intensity and the diamagnetic stored energy  $W_{dia}$ . The type-I ELM frequency is  $\sim 37$ [Hz] and  $\sim 45$ [Hz], and the ELM energy loss is  $\sim 89$ [kJ] and  $\sim 46$ [kJ] in the E49228 and E49229 plasmas, respectively.

loss becomes about half from  $\sim 89$ [kJ] to  $\sim 46$ [kJ]; the waveforms of these plasmas are shown in Fig.1.

Figure 2 shows the profiles of (a) the temperatures of the ion  $T_i$  and the electron  $T_e$ , (b) the electron number density  $n_e$  and the pressure  $p$ , (c) the rotation frequency  $\Omega$ , and (d) the parallel current density  $\langle \mathbf{j} \cdot \mathbf{B} \rangle / \langle B^2 \rangle$  and the safety factor  $q$ , respectively; these are the profiles just before the ELM crash. Here  $\rho_{vol.}$  is the radial coordinate defined as  $\rho_{vol.} \equiv \sqrt{V(\psi)/V_{tot.}}$ ,  $V$  is the volume in each flux surface,  $\psi$  is the poloidal flux normalized as  $\psi = 0$  ( $= 1$ ) at the axis (surface),  $V_{tot.}$  is the plasma total volume,  $\mathbf{j}$  is the plasma current density, and  $\mathbf{B}$  is the magnetic field. The  $\langle \mathbf{j} \cdot \mathbf{B} \rangle / \langle B^2 \rangle$  profile is obtained by estimating the bootstrap current, the neutral beam driven current, and the ohmic current with the ACCOME code [9]. The effective charge  $Z_{eff}$  values and the poloidal beta  $\beta_p$  values are (2.6, 0.85) and (2.8, 0.81) in the E49228 (CO.) and the E49229 (CTR.) plasmas, respectively. Hereafter, the E49228 and the E49229 plasmas are called as the CO. and CTR. plasmas. The profiles of  $T_i$  and  $n_e$  near the pedestal are measured with high spatial resolution by CXRS and LiBP [8]. Note that the  $T_i$  profiles outside the top of the  $T_i$  pedestal ( $\rho_{vol.} > 0.93$ ) are similar to each other but the  $n_e$  profile of the CTR. plasma is different from that of the CO. plasma; the  $n_e$  pedestal top and foot changes from  $\rho_{vol.} = 0.93$  and  $0.99$  (CO.) to  $0.91$  and  $0.96$  (CTR.). Such a difference of the  $n_e$  pedestal profile changes the position where the pressure gradient becomes maximum and the bootstrap current profile as shown in Figs.2 (b) and (d).

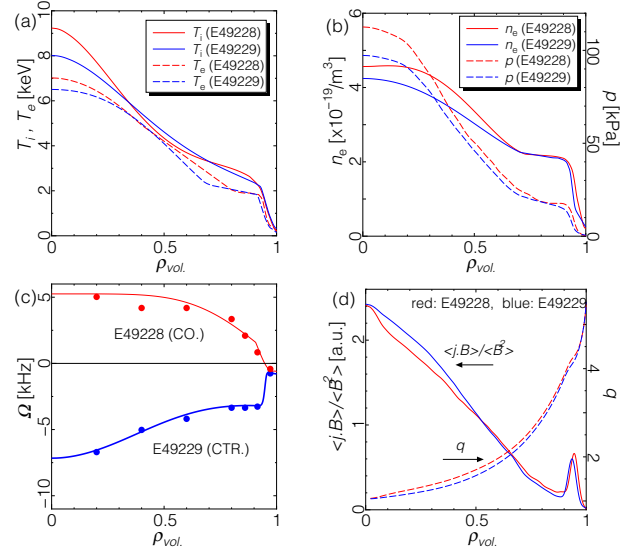


Fig. 2 Profiles of (a)  $T_i$  and  $T_e$ , (b)  $n_e$  and  $p$ , (c)  $\Omega$ , (d)  $\langle \mathbf{j} \cdot \mathbf{B} \rangle / \langle B^2 \rangle$  and  $q$ , in the E49228 (CO.) and the E49229 (CTR.) plasmas, respectively.

### 3. Stability analysis

#### 3.1 Stability analysis without a toroidal rotation

In this subsection, we investigate and compare the ideal MHD stability properties of the E49228 (CO.) and the E49229 (CTR.) plasmas without a toroidal rotation effect. This stability analysis is performed with the MARG2D code [10, 11] for the finite- $n$  MHD mode analysis and the BETA code [12] for the infinite- $n$  ballooning mode analysis, where  $n$  is the toroidal mode number. In this paper, the range of  $n$  of the analyzed MHD modes is from 1 to 30, and  $\infty$ .

The main object of the edge MHD stability analysis is to clarify the achievable pedestal pressure without instability. As the pedestal pressure becomes larger, the edge bootstrap current density also increases, and the edge MHD stability property is mainly determined by these equilibrium profiles. From this viewpoint, as mentioned in previous works [4, 11], the edge pedestal pressure gradient and the edge current density are the main parameters for the edge MHD stability analysis. In this paper, for varying these parameters, the pressure profile and the current profile near the pedestal are changed as

$$p_0(\psi) \propto p_{0-org}(\psi) \quad \dots (0 \leq \psi < 2\psi_{ped} - 1.0), \quad (1)$$

$$p_0(\psi) \propto p_{0-org}(\psi) \cdot (1.0 + C_{ped} \cdot \Psi) \quad \dots (2\psi_{ped} - 1.0 \leq \psi \leq 1.0), \quad (2)$$

$$\Psi \equiv \left( 1.0 - \left| \frac{\psi - \psi_{ped}}{1.0 - \psi_{ped}} \right|^2 \right)^2, \quad (3)$$

and

$$\langle \mathbf{j} \cdot \mathbf{B} \rangle / \langle B^2 \rangle \propto \langle \mathbf{j} \cdot \mathbf{B} \rangle / \langle B^2 \rangle_{org} + C_{BS} \langle \mathbf{j} \cdot \mathbf{B} \rangle / \langle B^2 \rangle_{BS}, \quad (4)$$

where  $p_0$  is the flux function part of the plasma pressure,  $p_{0-org}$  is the original  $p_0$  value of the reconstructed experimental data shown in Fig.2 (b),  $\psi_{ped}$  is the  $\psi$  value at the top of the pressure pedestal,  $\langle \mathbf{j} \cdot \mathbf{B} \rangle / \langle B^2 \rangle_{org}$  ( $\langle \mathbf{j} \cdot \mathbf{B} \rangle / \langle B^2 \rangle_{BS}$ ) is the original (bootstrap) ( $\mathbf{j} \cdot \mathbf{B} \rangle / \langle B^2 \rangle$ ) value calculated with the ACCOME code shown in Fig.2 (d), and  $C_{ped}$  ( $C_{BS}$ ) is the parameter for changing the pressure (current) profile near the pedestal. Note that since we fix the poloidal beta  $\beta_p$  and the plasma current  $I_p$ , the profiles of  $p_0$  and  $\langle \mathbf{j} \cdot \mathbf{B} \rangle / \langle B^2 \rangle$  are no longer same as the original profiles everywhere when  $C_{ped}, C_{BS} \neq 0$ . Also note that the plasma pressure is no longer the flux function in case that the plasma is rotating [13], and when the rotation is purely toroidal, the pressure can be written as

$$p = p_0(\psi) \exp \left[ M^2 \left( \frac{R^2}{R_0^2} - 1 \right) \right], \quad (5)$$

under the isothermal condition on each magnetic surface ( $T = T(\psi)$ ). Here  $M$  is the Mach number that is the ratio of the toroidal rotation velocity  $v_\phi = R_0 \Omega$  to the ion thermal velocity  $v_{th} = \sqrt{2T_i/m_i}$  as

$$M^2(\psi) \equiv \left( \frac{v_\phi}{v_{th}} \right)^2 = \frac{m_i R_0^2 \Omega^2}{2T_i}, \quad (6)$$

$m_i$  is the ion mass,  $R$  is the coordinate of the cylindrical coordinate system ( $R, Z, \phi$ ), and  $R_0$  is the major radius of the equilibrium.

Figure 3 shows the stability diagrams on the  $(j_{ped}, \alpha_{94})$  and  $(s_{94}, \alpha_{94})$  planes, where  $j_{ped}$  is the current density averaged over  $(2\psi_{ped} - 1.0) \leq \psi \leq 1.0$ ,  $\alpha$  is the normalized pressure gradient defined as  $\alpha \equiv -(\mu_0/2\pi^2)(dp_0/d\psi)(dV/d\psi)(VR/2\pi)^{0.5}$ ,  $\mu_0$  is the permeability in the vacuum,  $s$  is the magnetic shear defined as  $s \equiv 2V/q(dq/dV)$ , and the subscript 94 expresses the value at  $\psi = 0.94$ . Figures 3 (a) and (c) indicate that the CO. plasma is approximately on the stability boundary of the edge localized MHD mode without a toroidal rotation effect. In fact, the  $n = 12$  peeling-ballooning mode becomes marginally unstable by increasing  $C_{ped}$  to 0.1; this increment is thought to be within the error of the edge profile measurements.

On the other hand, as shown in Figs.3 (b) and (d), the CTR. plasma is far from the stability boundary without a toroidal rotation, and to make the plasma unstable, it is necessary to increase  $C_{ped} > 0.25$ . Since such a large increment in pressure is no longer within the margin of the error, this CTR. plasma without a toroidal rotation is stable against ideal MHD modes.

### 3.2 Stability analysis with a toroidal rotation

As mentioned in the previous subsection, the CTR. plasma without a toroidal rotation is stable against ideal MHD modes. However, as already mentioned, the type-I ELM was observed experimentally in this plasma. To understand this discrepancy, in this subsection, we investigate the toroidal rotation effect on the edge MHD stability

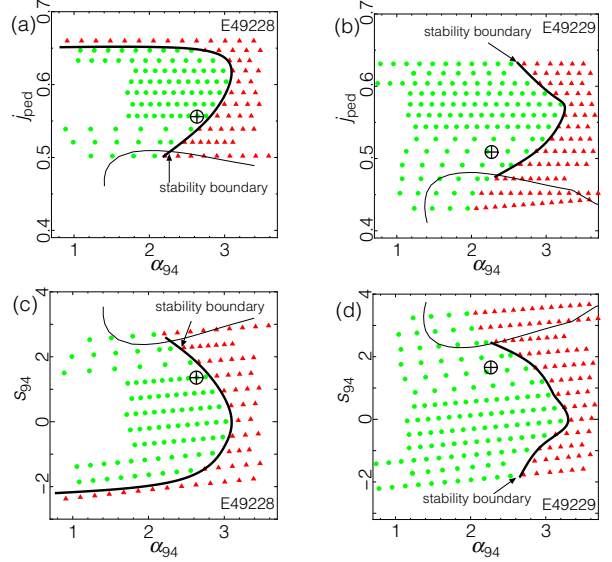


Fig. 3 Stability diagrams without the toroidal rotation effect on the  $(j_{ped}, \alpha_{94})$  plane of (a) the E49228 (CO.) and (b) the E49229 (CTR.) plasmas, and those on the  $(s_{94}, \alpha_{94})$  plane of (c) the CO. and (d) the CTR. plasmas, respectively. The (green) circle and (red) triangle mean stable and unstable for the finite- $n$  MHD modes, the solid line shows the stability boundary determined by the finite- $n$  MHD modes and the infinite- $n$  ballooning mode, and the target expresses the equilibrium values observed experimentally. As shown in these figures, the CO. plasma is approximately on the stability boundary of the edge localized MHD mode, but the CTR. plasma is far from this stability boundary.

in these plasmas. The numerical analysis including a rotation effect is performed with the MINERVA code [14], which solves the Frieman-Rosenbluth equation [15], the linear ideal MHD equation with flow. As mentioned in the previous subsection, since the CO. plasma becomes marginally unstable by increasing  $C_{ped}$  to 0.1, we investigate the toroidal rotation effect on the edge MHD stability under the condition  $C_{ped} = 0.1$  in both CO. and CTR. plasmas. Note that MARG2D solves the eigenvalue problem associated with the two-dimensional Newcomb equation [10]

$$\mathcal{N}Y = -\lambda_0 \mathcal{R}Y, \quad (7)$$

and realizes to calculate the eigenvalue numerically even when the plasma is stable ( $\lambda_0 > 0$ ), where  $\mathcal{N}$  is the Newcomb operator,  $Y \equiv r\xi$ ,  $r$  is the radial coordinate,  $\xi$  is the plasma displacement,  $\lambda_0$  is the eigenvalue, and  $\mathcal{R}$  is the weight function defined in Ref. [10]. This advantage realizes to identify the stability boundary of the MHD mode as the contour of  $\lambda_0 = 0$  in the static equilibrium case.

However, since the MINERVA code solves the initial

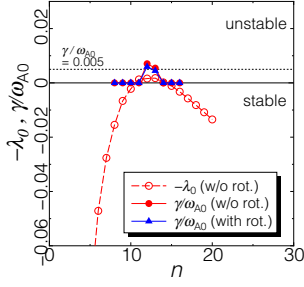


Fig. 4 Dependences of  $-\lambda_0$  and  $\gamma/\omega_{A0}$  on  $n$  in the CO. plasma with and without the toroidal rotation when  $C_{ped} = 0.1$ . The toroidal rotation has little impact on this CO. plasma, and the  $n = 12$  mode is marginally unstable.

value problem of the Frieman-Rosenbluth equation,

$$\rho \frac{\partial^2 \xi}{\partial t^2} + 2\rho(\mathbf{u} \cdot \nabla) \frac{\partial \xi}{\partial t} + \rho(\mathbf{u} \cdot \nabla)(\mathbf{u} \cdot \nabla)\xi = \mathbf{F}(\xi) = \mathbf{F}_s(\xi) + \mathbf{F}_d(\xi), \quad (8)$$

$$\mathbf{F}_s \equiv \nabla [\xi \cdot \nabla p + \Gamma p \nabla \cdot \xi] + (\nabla \times \mathbf{Q}) \times \mathbf{B} + \mathbf{j} \times \mathbf{Q}, \quad (9)$$

$$\mathbf{F}_d \equiv \nabla \cdot [\rho \xi (\mathbf{u} \cdot \nabla) \mathbf{u} - \rho \mathbf{u} (\mathbf{u} \cdot \nabla) \xi] + \rho(\mathbf{u} \cdot \nabla)(\mathbf{u} \cdot \nabla)\xi, \quad (10)$$

this code cannot identify strictly the marginal condition ( $\gamma/\omega_{A0} = 0$ ). Here  $\rho$  is the plasma mass density,  $\mathbf{u}$  is the equilibrium rotation velocity,  $\mathbf{F}$  is the force operator,  $\mathbf{F}_s$  is the force operator that has the same vector form as that in static equilibrium case,  $\mathbf{F}_d$  is the sum of the remaining force terms that express the rotation effect on the force operator  $\mathbf{F}$ ,  $\mathbf{Q}$  is the fluctuation of the magnetic field given by

$$\mathbf{Q} \equiv \nabla \times (\xi \times \mathbf{B}), \quad (11)$$

and  $\omega_{A0}$  is the toroidal Alfvén frequency at the axis. Accordingly, the stability boundary is determined by extrapolating  $\gamma$  into 0 from computable (positive)  $\gamma$  values in case that the equilibrium rotates. Note that one of  $\gamma/\omega_{A0}$  used for extrapolating is enough small ( $\sim 5.0 \times 10^{-3}$ ) to identify the stability boundary with high accuracy. In this paper, since we assume that the plasma rotation is purely in the toroidal direction,  $\mathbf{u}$  can be written as  $\mathbf{u} = R^2 \Omega \nabla \phi$ .

Figure 4 shows the  $n$  dependences of  $-\lambda_0$  and  $\gamma/\omega_{A0}$  in the CO. plasmas with and without the toroidal rotation whose profile is shown in Fig.2 (c). As shown in this figure, the rotation profile of the CO. plasma has little impact on the edge MHD stability, and the  $n = 12$  mode is marginally unstable as in the static case.

Next, we investigate the rotation effect on the edge MHD stability in the CTR. plasma. In this analysis, we investigate not only the  $n$  dependence but also the rotation dependence of  $\gamma/\omega_{A0}$  by changing the rotation profile from rot.1 (original profile shown in Fig.2 (c)) to rot.2 and rot.3 shown in Fig.5 (a). These rot.2 and rot.3 profiles are determined by increasing the  $\Omega$  value at  $\rho_{vol.} = 0.92$  as 1.1

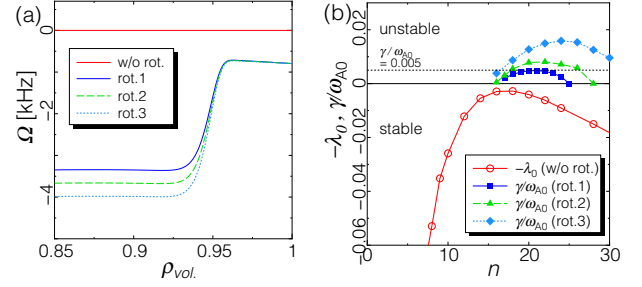


Fig. 5 (a) Enlarged view of  $\Omega$  of the CTR. plasma. To investigate the rotation effect on the MHD stability in the CTR. plasma, three kinds of the rotation profile (rot.1, rot.2, rot.3) are used for the stability analysis. (b) Dependences of  $-\lambda_0$  and  $\gamma/\omega_{A0}$  on  $n$  in the CTR. plasma, whose rotation profile is  $\Omega = 0$ , rot.1, rot.2, and rot.3, respectively. The toroidal rotation of CTR. plasma (rot.1) destabilizes the MHD mode, and the  $n = 20$  mode becomes marginally unstable.

and 1.2 times larger than rot.1, respectively. Figure 5 (b) shows the  $n$  dependence of  $-\lambda_0$  and  $\gamma/\omega_{A0}$  in the CTR. plasma. As shown in this figure, though the CTR. plasma without rotation is stable against ideal MHD modes, the toroidal rotation of CTR. plasma (rot.1) destabilizes the MHD mode, and the  $n = 20$  mode becomes marginally unstable. Moreover, by increasing the rotation frequency, not only the growth rate but also the  $n$  number of the most unstable mode become larger; for example, when the rotation profile is rot.3, the  $n = 26$  mode is the most unstable mode, whose  $\gamma/\omega_{A0}$  approaches to 0.02.

Based on these numerical results, we investigate the stability boundary of both the CTR. plasmas with the toroidal rotation shown in Fig.2 (c). Figure 6 shows the stability diagram on the  $(j_{ped}, \alpha_{94})$  and the  $(s_{94}, \alpha_{94})$  planes in the CTR. plasma with and without the toroidal rotation. As shown in these figures, by adding the toroidal rotation, the stability boundary moves to the smaller  $\alpha_{94}$  side, and as the result, the threshold pressure gradient becomes smaller from  $\alpha_{94-max} \simeq 2.77$  to  $\simeq 2.28$  under the same  $\langle \mathbf{j} \cdot \mathbf{B} \rangle / \langle B^2 \rangle \simeq 0.5$  condition. Moreover, the  $n$  number of the MHD modes, which determines the stability boundary, becomes larger as the rotation frequency increases, and the destabilizing effect of the toroidal rotation becomes stronger as the  $n$  number of the MHD mode increases. For example, on the stability boundary at  $\langle \mathbf{j} \cdot \mathbf{B} \rangle / \langle B^2 \rangle \simeq 0.5$ , the  $n$  number of the MHD mode changes from 16 to 20 by adding the toroidal rotation. This result is consistent with the results of the qualitative and quantitative analyses of the rotation and the rotation shear effects on the edge MHD stability in Refs. [5, 7, 14], and resolves the discrepancy mentioned at the front of this subsection.

## 4. Summary

We analyze numerically the toroidal rotation effect on the type-I ELM property by comparing the stability prop-

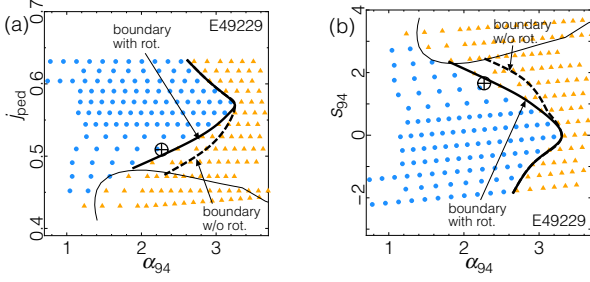


Fig. 6 Stability diagrams on (a) the  $(j_{ped}, \alpha_{94})$  and (b) the  $(s_{94}, \alpha_{94})$  plane of the CTR. plasma, respectively. The (blue) circle and (orange) triangle means stable and unstable for the finite- $n$  MHD modes, the solid line shows the stability boundary of the finite- $n$  MHD modes and the infinite- $n$  ballooning mode in the CTR. plasma with the rotation profile rot.1., the broken line shows the stability boundary of the finite- $n$  MHD modes in the CTR. plasma without the rotation., and the target expresses the equilibrium values observed experimentally. By adding the toroidal rotation, the stability boundary moves to the smaller  $\alpha_{94}$  side, and as the result, the threshold pressure gradient becomes smaller from  $\alpha_{94-max} \simeq 2.77$  to  $\simeq 2.28$  under the same  $(\mathbf{j} \cdot \mathbf{B})/\langle B^2 \rangle \simeq 0.5$  condition.

erties between the E49228 and the E49229 type-I ELMy H-mode plasmas in JT-60U, which are rotating in the co- and ctr- directions to the plasma current, respectively. As the result of the stability analysis, we clarify that the toroidal rotation has little impact on the MHD stability in the E49228 co-rotating plasma, and this plasma just before the ELM is approximately on the stability boundary of the edge localized MHD mode in each static and rotating case. On the other hand, the E49229 ctr-rotating plasma is far from the stability boundary under the static assumption. In this ctr-rotating plasma, the toroidal rotation destabilizes the edge MHD mode, and reduces the stability limit of the pressure gradient near the pedestal. As the result of this destabilization, this ctr-rotating plasma just before ELM is also considered as the marginally unstable against edge MHD mode.

As mentioned in the introduction, we have reported that the destabilization of edge localized MHD mode by the toroidal rotation with shear is mainly caused by the difference between the frequency of the eigenmode and the toroidal rotation frequency; this mechanism is identified by defining the energy in Ref. [7] as

$$\delta W_{rot.-n^2} \equiv n^2 \langle \xi | \rho (\omega^2 - \Omega^2) | \xi \rangle. \quad (12)$$

This energy is proportional to  $n^2$ , and increases as the rotation shear becomes larger. By comparing the rotation profiles between the E49228 and the E49229 plasmas, the rotation shear near the pedestal in the E49229 plasma is locally more than twice that in the E49228 one. Moreover, as mentioned in Subsec.3.2, the  $n$  number of the marginally unstable mode is 20 in the E49229 plasma, which is larger than that in the E49228 plasma ( $= 12$ ). These results im-

ply that the destabilizing effect by the toroidal rotation with shear is more effective in the E49229 plasma than that in the E49228 plasma. Actually, at the marginally unstable point near the operation point on the  $(j_{ped}, \alpha_{94})$  diagram, the  $\delta W_{rot.-n^2}/\delta W_K$  value at  $(j_{ped}, \alpha_{94}) = (0.50, 2.28)$  is  $-4.95 \times 10^{-4}$  in the E49229 plasma, and this is about twice as large as that ( $= -2.52 \times 10^{-4}$ ) at  $(j_{ped}, \alpha_{94}) = (0.55, 2.75)$  in the E49228 plasma, where  $\delta W_K \equiv \langle \xi | \rho | \xi \rangle$  is the kinetic energy. The more detailed discussion about the destabilizing mechanism is reported in Ref. [7].

In this paper, since the measurements with high spatial resolution is necessary for the edge MHD stability analysis of the experimental results, and the physics of the type-I ELM is relatively well-understood qualitatively and quantitatively, we select the E49228 and the E49229 type-I ELMy H-mode plasmas as the objects of the numerical analysis. To understand the toroidal rotation effect on the ELM phenomena in more detail, it is important to understand this effect on not only the type-I ELM but also the other ELMs. Particularly, as discussed in Ref. [2], the grassy ELM strongly depends on the toroidal rotation frequency, and since the ELM energy loss of the grassy ELM is much smaller than that of the type-I ELM, this grassy ELM is thought to be more favorable than the type-I ELM for ITER and future devices. From this viewpoint, we will investigate the toroidal rotation effect on the grassy ELM and will report in near future.

## Acknowledgments

The authors are grateful to Dr. M. Mori, Dr. T. Ozeki for their support. This work was partially supported by the Ministry of Education, Science, Sports and Culture, Grant-in-Aid for Young Scientists (B), 2009, 21760698.

## References

- [1] E. J. Doyle *et al.*, Nucl. Fusion **47**, S85 (2007).
- [2] N. Oyama *et al.*, Plasma Phys. Control. Fusion **49**, 249 (2007).
- [3] H. Urano *et al.*, Nucl. Fusion **47**, 706 (2007).
- [4] P. B. Snyder *et al.*, Phys. Plasmas **9**, 2037 (2002).
- [5] N. Aiba, S. Tokuda, M. Furukawa, N. Oyama, and T. Ozeki, Nucl. Fusion **49**, 065015 (2009).
- [6] P. B. Snyder *et al.*, Nucl. Fusion **47**, 961 (2007).
- [7] N. Aiba, M. Furukawa, M. Hirota, and S. Tokuda, to be published in Nucl. Fusion.
- [8] A. Kojima *et al.*, Nucl. Fusion **49**, 115008 (2009).
- [9] K. Tani, M. Azumi, and R. S. J. Devoto, J. Comput. Phys. **98**, 332 (1992).
- [10] S. Tokuda and T. Watanabe, Phys. Plasmas **6**, 3012 (1999).
- [11] N. Aiba, S. Tokuda, T. Ishizawa, and M. Okamoto, Comput. Phys. Commun. **175**, 269 (2006).
- [12] M. Azumi *et al.*, in *Proc. 6th Int. Conf. Plasma Phys., Lausanne*, volume 1, page 200, Brussels: CEC, 1984.
- [13] T. Takeda and S. Tokuda, J. Comput. Phys. **93**, 1 (1991).
- [14] N. Aiba, S. Tokuda, M. Furukawa, P. B. Snyder, and M. S. Chu, Comput. Phys. Commun. **180**, 1282 (2009).
- [15] E. Frieman and M. Rotenberg, Rev. Mod. Phys. **32**, 898 (1960).